Extended Higgs Sectors at Future e^+e^- Colliders

Duarte Azevedo[1][*], Pedro Ferreira[1,2][†], Margarete Mühlleitner[3][‡],
Rui Santos[1,2,4][§], Jonas Wittbrodt[5][¶]

[1] *Centro de Física Teórica e Computacional, Faculdade de Ciências,*
Universidade de Lisboa, Campo Grande, Edifício C8 1749-016 Lisboa, Portugal

[2] *ISEL - Instituto Superior de Engenharia de Lisboa,*
Instituto Politécnico de Lisboa 1959-007 Lisboa, Portugal

[3] *Institute for Theoretical Physics, Karlsruhe Institute of Technology,*
76128 Karlsruhe, Germany

[4] *LIP, Departamento de Física, Universidade do Minho, 4710-057 Braga, Portugal*

[5] *Deutsches Elektronen-Synchrotron DESY, Notkestraße 85, 22607 Hamburg, Germany*

Abstract

We compare several Beyond the Standard Model (SM) models with extended Higgs sectors. The models comprise the SM extended by a complex singlet field (CxSM), the 2-Higgs-Doublet Model with a CP-conserving (2HDM) and a CP-violating violating (C2HDM) scalar sector, the singlet extension of the 2- Higgs-Doublet Model (N2HDM), and the Next-to-Minimal Supersymmetric SM extension (NMSSM). All the above models have at least three neutral bosons, with one being the 125 GeV Higgs boson. This common feature allows us to compare the production and decay rates of the other two scalars. Using a set of benchmark centre-of-mass energies and luminosities, we discuss which models can be probed and if it is possible to distinguish between them. Taking into account the expected accuracy in the measurements of the 125 GeV Higgs couplings, for the different CLIC configurations, we discuss possible deviations from its SM character, focusing on the CP-violating or the non-doublet character of the 125 GeV Higgs boson. The expected precision at electron-positron colliders will certainly contribute to a clearer picture of the nature of the Higgs boson.

---

[*]E-mail: `fc40613@alunos.fc.ul.pt`

[†]E-mail: `pmmferreira@fc.ul.pt`

[‡]E-mail: `milada.muehlleitner@kit.edu`

[§]E-mail: `rasantos@fc.ul.pt`

[¶]E-mail: `jonas.wittbrodt@desy.de`

1   Introduction

The discussion of physics in future colliders has recently become a very important issue due to the absence of hints of New Physics beyond the Standard Model (BSM). In fact, although a Higgs boson has been discovered by the LHC experiments ATLAS [1] and CMS [2], no other solid hints of New Physics have been reported by the LHC collaborations until now. On the contrary, the LHC results point to a SM-like Higgs boson with couplings to the remaining SM particles well within the SM expectations.

In this work we analyse several extensions of the SM: the SM extended by a complex singlet field (CxSM), the 2-Higgs-Doublet Model with a CP-conserving (2HDM) and a CP-violating violating (C2HDM) scalar sector, the singlet extension of the 2-Higgs-Doublet Model (N2HDM), and the Next-to-Minimal Supersymmetric SM extension (NMSSM). The models have in common the presence of at least three neutral bosons (one being the 125 GeV Higgs boson), which allow for the comparison of the production and decay rates of the other two scalars.

We focus mainly on two different issues. The first part of the work is about the nature of the discovered Higgs boson. The SM 125 GeV scalar originates from an $SU(2)$ doublet. When other fields are added to the SM content, mixing between fields from doublets and/or singlets takes place. The Higgs boson can acquire extra singlet or pseudoscalar components from the mixing. So the question is what can an electron-positron collider such as CLIC tell us about the amount of mixing in the 125 GeV Higgs boson. The second part of the work focuses on the two non-125 GeV Higgs bosons and on the possibility to distinguish the different models if a new scalar is found. The issue addressed is whether we are able to disentangle the models based on Higgs rate measurements. We hope that we can shed some light on the relevance of a future electron-positron collider for BSM Higgs searches.

In section 2 we briefly introduce the models and the scan over their parameter spaces. Section 3 is devoted to the nature of the 125 GeV Higgs boson after CLIC and in section 4 we compare the signal rates of the two non-SM-like Higgs bosons within the different models. Our conclusions are given in section 5.

2   Short Description of the Models

The models discussed in this work were introduced in detail in [3]. Here, we will only give their potentials, the particle spectrum and the independent parameters of the models.

- **Complex Singlet Extension of the SM (CxSM)**

  The model is an extension of the SM through the addition of a complex scalar singlet. The potential has a softly broken global $U(1)$ symmetry and is given by

  $$V = \frac{m^2}{2}H^\dagger H + \frac{\lambda}{4}(H^\dagger H)^2 + \frac{\delta_2}{2}H^\dagger H|\mathbb{S}|^2 + \frac{b_2}{2}|\mathbb{S}|^2 + \frac{d_2}{4}|\mathbb{S}|^4 + \left(\frac{b_1}{4}\mathbb{S}^2 + a_1\mathbb{S} + c.c.\right), \quad (2.1)$$

  where $\mathbb{S} = S + iA$ is a hypercharge zero scalar and the soft breaking terms are written in parenthesis. We further impose invariance under $\mathbb{S} \to \mathbb{S}^*$ (or $A \to -A$), and so a_1 and b_1 are real. We work in the broken phase where the three CP-even scalars mix. The mass eigenstates for these scalars are denoted by H_i and are obtained from the gauge eigenstates

via the rotation matrix R parametrised as

$$R = \begin{pmatrix} c_1 c_2 & s_1 c_2 & s_2 \\ -(c_1 s_2 s_3 + s_1 c_3) & c_1 c_3 - s_1 s_2 s_3 & c_2 s_3 \\ -c_1 s_2 c_3 + s_1 s_3 & -(c_1 s_3 + s_1 s_2 c_3) & c_2 c_3 \end{pmatrix} , \tag{2.2}$$

where we have defined $s_i \equiv \sin \alpha_i$ and $c_i \equiv \cos \alpha_i$, and

$$-\frac{\pi}{2} \le \alpha_i < \frac{\pi}{2} . \tag{2.3}$$

The masses of the neutral Higgs bosons are ordered as $m_{H_1} \le m_{H_2} \le m_{H_3}$. We choose as input parameters the set

$$\alpha_1 , \quad \alpha_2 , \quad \alpha_3 , \quad v , \quad v_S , \quad m_{H_1} \quad \text{and} \quad m_{H_3} , \tag{2.4}$$

and the remaining parameters are determined internally in `ScannerS` [4, 5] fulfilling the minimum conditions of the vacuum.

All couplings of each Higgs boson H_i to SM particles are rescaled by a common factor R_{i1}. Expressions for all couplings are available in [6] and the Higgs branching ratios, including the state-of-the art higher order QCD corrections and possible off-shell decays can be obtained from `sHDECAY` [6][1] which implements the CxSM and also the RxSM both in their symmetric and broken phases in `HDECAY` [7, 8].

- **Two-Higgs Doublet Model - Real (2HDM) and Complex (C2HDM)**

  The model is an extension of the SM by a second scalar doublet. The potential is invariant under the softly broken $\mathbb{Z}_2$ transformation $\Phi_1 \to \Phi_1$ and $\Phi_2 \to -\Phi_2$ and can be written as

$$\begin{aligned} V &= m_{11}^2 |\Phi_1|^2 + m_{22}^2 |\Phi_2|^2 - m_{12}^2 (\Phi_1^\dagger \Phi_2 + h.c.) + \frac{\lambda_1}{2} (\Phi_1^\dagger \Phi_1)^2 + \frac{\lambda_2}{2} (\Phi_2^\dagger \Phi_2)^2 \\ &\quad + \lambda_3 (\Phi_1^\dagger \Phi_1)(\Phi_2^\dagger \Phi_2) + \lambda_4 (\Phi_1^\dagger \Phi_2)(\Phi_2^\dagger \Phi_1) + [\frac{\lambda_5}{2} (\Phi_1^\dagger \Phi_2)^2 + h.c.] . \end{aligned} \tag{2.5}$$

  The extension of the $\mathbb{Z}_2$ symmetry to the fermions guarantees that the model is free from tree-level flavour changing neutral currents (FCNC). The potential is CP-conserving and referred to as 2HDM if all parameters of the potential and the VEVs are real. The potential is CP-violating if the VEVs are real but m_{12}^2 and λ_5 are complex and we call it C2HDM [9]. Both models have three neutral scalars and two charged Higgs bosons. In the 2HDM the neutral scalars are h and H, the lighter and the heavier CP-even states, while A is the CP-odd state. In the C2HDM we define three Higgs mass eigenstates H_i $(i = 1, 2, 3)$ with no definite CP that are ordered as $m_{H_1} \le m_{H_2} \le m_{H_3}$. The rotation matrix R that diagonalises the mass matrix is parametrised in Eqs. (2.2) and (2.3).

  The 2HDM has 8 independent parameters while the C2HDM has 9 independent parameters. We define $v = \sqrt{v_1^2 + v_2^2} \approx 246$ GeV and $\tan \beta = v_2/v_1$ for both versions of the model. For the 2HDM we choose the independent parameters

$$v , \quad \tan \beta , \quad \alpha , \quad m_h , \quad m_H , \quad m_A , \quad m_{H^\pm} \quad \text{and} \quad m_{12}^2 , \tag{2.6}$$

---

[1]The program `sHDECAY` can be downloaded from the url: `itp.kit.edu/~maggie/sHDECAY`.

while for the C2HDM we use [10]

$$v , \quad \tan\beta , \quad \alpha_{1,2,3} , \quad m_{H_i} , \quad m_{H_j} , \quad m_{H^\pm} \quad \text{and} \quad Re(m_{12}^2) , \tag{2.7}$$

where m_{H_i} and m_{H_j} denote any two of the three neutral Higgs bosons. The remaining mass is obtained from the other parameters [10].

All Higgs branching ratios, including the state-of-the art higher order QCD corrections and possible off-shell decays can be obtained from `C2HDM_HDECAY` [11][2] which is an implementation of the C2HDM in `HDECAY` [7, 8]. The complete set of Feynman rules for the C2HDM is available at:

<div align="center">porthos.tecnico.ulisboa.pt/arXiv/C2HDM/</div>

.

The 2HDM branching ratios are part of the `HDECAY` release (see [8, 12] for details).

- **Next-to-Two-Higgs Doublet Model (N2HDM)**

The model [13] is an extension of the SM by a doublet and a real singlet. The potential is invariant under two discrete $\mathbb{Z}_2$ symmetries, $\Phi_1 \to \Phi_1$, $\Phi_2 \to -\Phi_2$, $\Phi_S \to \Phi_S$ (as in the 2HDM, to avoid tree-level FCNCs), softly broken by m_{12}^2, and $\Phi_1 \to \Phi_1$, $\Phi_2 \to \Phi_2$, $\Phi_S \to -\Phi_S$, which is not explicitly broken. The most general form of this scalar potential is

$$
\begin{aligned}
V &= m_{11}^2|\Phi_1|^2 + m_{22}^2|\Phi_2|^2 - m_{12}^2(\Phi_1^\dagger\Phi_2 + h.c.) + \frac{\lambda_1}{2}(\Phi_1^\dagger\Phi_1)^2 + \frac{\lambda_2}{2}(\Phi_2^\dagger\Phi_2)^2 \\
&\quad + \lambda_3(\Phi_1^\dagger\Phi_1)(\Phi_2^\dagger\Phi_2) + \lambda_4(\Phi_1^\dagger\Phi_2)(\Phi_2^\dagger\Phi_1) + \frac{\lambda_5}{2}[(\Phi_1^\dagger\Phi_2)^2 + h.c.] \\
&\quad + \frac{1}{2}m_S^2\Phi_S^2 + \frac{\lambda_6}{8}\Phi_S^4 + \frac{\lambda_7}{2}(\Phi_1^\dagger\Phi_1)\Phi_S^2 + \frac{\lambda_8}{2}(\Phi_2^\dagger\Phi_2)\Phi_S^2 .
\end{aligned}
\tag{2.8}
$$

This particular version of the N2HDM is CP-conserving and the particle spectrum consists of three CP-even scalars, one CP-odd scalar and a pair of charged Higgs bosons. The CP-even states are obtained from the gauge eigenstates via the same rotation matrix R defined in Eqs. (2.2) and Eq. (2.3). These states are denoted by H_1, H_2 and H_3 and are ordered as $m_{H_1} < m_{H_2} < m_{H_3}$. The 12 independent parameters are

$$\alpha_1 , \quad \alpha_2 , \quad \alpha_3 , \quad t_\beta , \quad v , \quad v_s , \quad m_{H_{1,2,3}} , \quad m_A , \quad m_{H^\pm} , \quad m_{12}^2 . \tag{2.9}$$

All Higgs branching ratios, including the state-of-the art higher order QCD corrections and possible off-shell decays can be obtained from `N2HDECAY`[3] [14].

- **The Next-to-Minimal Supersymmetric Standard Model (NMSSM)**

The NMSSM is obtained by extending the two Higgs doublet superfields $\hat{H}_u$ and $\hat{H}_d$ in the Minimal Supersymmetric extension (MSSM) by a complex superfield $\hat{S}$. The NMSSM Higgs potential is derived from the superpotential, the soft SUSY breaking Lagrangian and the D-term contributions. In terms of the hatted superfields, the scale-invariant NMSSM superpotential is given by

$$\mathcal{W} = \lambda\widehat{S}\widehat{H}_u\widehat{H}_d + \frac{\kappa}{3}\widehat{S}^3 + h_t\widehat{Q}_3\widehat{H}_u\widehat{t}_R^c - h_b\widehat{Q}_3\widehat{H}_d\widehat{b}_R^c - h_\tau\widehat{L}_3\widehat{H}_d\widehat{\tau}_R^c , \tag{2.10}$$

---

[2]The program `C2HDM_HDECAY` can be downloaded from `itp.kit.edu/~maggie/C2HDM`.
[3]The program `N2HDECAY` is available at `gitlab.com/jonaswittbrodt/N2HDECAY` and based on `HDECAY` [7, 8].

where for simplicity only the third generation fermion superfields have been included. Here $\widehat{Q}_3$ and $\widehat{L}_3$ denote the left-handed doublet quark and lepton superfields, respectively, and $\widehat{t}_R^c, \widehat{b}_R^c$ and $\widehat{\tau}_R^c$ the right-handed singlet quark and lepton superfields each. The soft SUSY breaking Lagrangian is given by the mass terms for the Higgs and the sfermion fields, built from the complex scalar components of the superfields,

$$
\begin{aligned}
-\mathcal{L}_{\mathrm{mass}} &= m_{H_u}^2 |H_u|^2 + m_{H_d}^2 |H_d|^2 + m_S^2 |S|^2 \\
&+ m_{\tilde{Q}_3}^2 |\tilde{Q}_3^2| + m_{\tilde{t}_R}^2 |\tilde{t}_R^2| + m_{\tilde{b}_R}^2 |\tilde{b}_R^2| + m_{\tilde{L}_3}^2 |\tilde{L}_3^2| + m_{\tilde{\tau}_R}^2 |\tilde{\tau}_R^2| ,
\end{aligned} \tag{2.11}
$$

the contribution from the trilinear soft SUSY breaking interactions between the sfermions and the Higgs fields

$$
\begin{aligned}
-\mathcal{L}_{\mathrm{tril}} &= \lambda A_\lambda H_u H_d S + \frac{1}{3}\kappa A_\kappa S^3 + h_t A_t \tilde{Q}_3 H_u \tilde{t}_R^c - h_b A_b \tilde{Q}_3 H_d \tilde{b}_R^c \\
&- h_\tau A_\tau \tilde{L}_3 H_d \tilde{\tau}_R^c + \text{h.c.} ,
\end{aligned} \tag{2.12}
$$

where the A's denote the soft SUSY breaking trilinear couplings, and the contribution from the gaugino mass parameters $M_{1,2,3}$ of the bino ($\tilde{B}$), winos ($\tilde{W}$) and gluinos ($\tilde{G}$), respectively,

$$
-\mathcal{L}_{\mathrm{gauginos}} = \frac{1}{2}\left[M_1 \tilde{B}\tilde{B} + M_2 \sum_{a=1}^{3} \tilde{W}^a \tilde{W}_a + M_3 \sum_{a=1}^{8} \tilde{G}^a \tilde{G}_a + \text{h.c.} \right] . \tag{2.13}
$$

The soft terms are assumed to be non-universal at the GUT scale.

The particle spectrum of the NMSSM contains three CP-even Higgs mass eigenstates H_i ($i = 1, 2, 3$), with $m_{H_1} \leq m_{H_2} \leq m_{H_3}$, two CP-odd mass eigenstates A_1 and A_2, with $m_{A_1} \leq m_{A_2}$, and a pair of charged Higgs bosons. Using the minimisation conditions we can parametrise the tree-level NMSSM Higgs sector by six independent parameters, chosen as

$$
\lambda , \; \kappa , \; A_\lambda , \; A_\kappa, \; \tan\beta = v_u/v_d \quad \text{and} \quad \mu_{\mathrm{eff}} = \lambda v_s/\sqrt{2} . \tag{2.14}
$$

The sign conventions are such that λ and $\tan\beta$ are positive, whereas $\kappa, A_\lambda, A_\kappa$ and μ_{eff} are allowed to have both signs. Due to the corrections to the SM-like Higgs boson mass, necessary to shift it to the measured 125 GeV, also the soft SUSY breaking mass terms for the scalars and the gauginos as well as the trilinear soft SUSY breaking couplings contribute to the Higgs sector. We use the NMSSMTools package [15–20] to calculate the Higgs masses and decay widths including the relevant higher order corrections. We have cross-checked these results against NMSSMCALC [21].

We have performed parameter scans in these models by varying the input parameters through the phenomenologically interesting ranges. Our scans take into account all applicable theoretical and experimental constraints. The parameter ranges and details on the applied constraints can be found in [3]. Note that the 125 GeV Higgs boson can be the lightest as well as a heavier scalar. This possibility is not excluded in any of the models.

Parameter	Relative precision [22, 23]		
	350 GeV 500 fb^{-1}	+1.4 TeV +1.5 ab^{-1}	+3.0 TeV +2.0 ab^{-1}
κ_{HZZ}	0.43%	0.31%	0.23%
κ_{HWW}	1.5%	0.15%	0.11%
κ_{Hbb}	1.7%	0.33%	0.21%
κ_{Hcc}	3.1%	1.1%	0.75%
κ_{Htt}	−	4.0%	4.0%
$\kappa_{H\tau\tau}$	3.4%	1.3%	<1.3%
$\kappa_{H\mu\mu}$	−	14%	5.5%
κ_{Hgg}	3.6%	0.76%	0.54%
$\kappa_{H\gamma\gamma}$	−	5.6%	< 5.6%

Table 1: Results of the model-dependent global Higgs fit on the expected precisions of the κ_{Hii} (see text). Entries marked "−" cannot be measured with sufficient precision at the given energy. We call the first (350 GeV) scenario $Sc1$, the second (1.4 TeV) $Sc2$ and the third (3.0 TeV) $Sc3$.

3 Phenomenological Analysis

3.1 The Nature of the 125 GeV Higgs Boson after CLIC

Over the last years, predictions for the measurement of the Higgs couplings to fermions and gauge bosons at CLIC were made for several benchmark energies and luminosities. Table 1 shows the expected precision in the measurement of the Higgs couplings from [22] (see [22, 23] for details). The κ_{Hii} are defined as

$$\kappa_{Hii} = \sqrt{\frac{\Gamma_{Hii}^{BSM}}{\Gamma_{Hii}^{SM}}} \, , \tag{3.15}$$

which at tree-level is just the ratio of the Higgs coupling in the BSM model and the corresponding SM Higgs coupling. We call the three benchmarks scenarios $Sc1$ (350 GeV), $Sc2$ (1.4 TeV) and $Sc3$ (3.0 TeV). With these predictions we now study the effect on the parameter space of each model presented in the previous section. This will tell us how much an extra component from either a singlet (or more singlets) or a doublet contributes to the h_{125} scalar boson. Clearly, if no new scalar is discovered one can only set bounds on the amount of mixing with extra fields. In the case of a CP-violating model it is possible to set a bound on the ratio of pseudoscalar to scalar Yukawa couplings, where there is an important interplay with the results from measurements of electric dipole moments (EDMs) . The results presented in this section assume that the measured central value is the SM expectation, meaning that all κ_{Hii} in Table 1 have a central value of 1. If significant deviations from the SM predicted values are found the data has to be reinterpreted for each model.

Starting with the simplest extension, the CxSM, there are either one or two singlet components that mix with the real neutral part of the Higgs doublet. The admixture is given by the sum of the squared mixing matrix elements corresponding to the real and complex singlet parts, *i.e.*

$$\Sigma_i^{\text{CxSM}} = (R_{i2})^2 + (R_{i3})^2 \, , \tag{3.16}$$

with the matrix R defined in Eq. (2.2)[4]. All Higgs couplings to SM particles are rescaled by a common factor. Therefore, we only need to consider the most accurate Higgs coupling measurement to get the best constraints on the Higgs admixture. The maximum allowed singlet admixture is given by the lower bound on the global signal strength μ which at present is

$$\Sigma^{\mathrm{CxSM}}_{\mathrm{max\ LHC}} \approx 1 - \mu_{\min} \approx 11\% \,. \tag{3.17}$$

In CLIC $Sc1$ the most accurate measurement is for the scaled coupling κ_{HZZ}, which would give

$$\Sigma^{\mathrm{CxSM}}_{\mathrm{max\ CLIC@350GeV}} \approx 0.85\% \,, \tag{3.18}$$

while for $Sc3$ one would obtain, from κ_{HWW},

$$\Sigma^{\mathrm{CxSM}}_{\mathrm{max\ CLIC@3TeV}} \approx 0.22\% \,. \tag{3.19}$$

This implies, for this particular kind of extensions, that the chances of finding a new scalar are reduced due to the orthogonality of the R matrix. Note that in the limit of exact zero singlet component the singlet fields do not interact with the SM particles. The results for a real singlet are similar, with the bound being exactly the same but with a two by two orthogonal matrix replacing R. In this case it is exactly the value 0.22% that multiplies all production cross sections of the non-SM Higgs boson, after CLIC@3TeV.
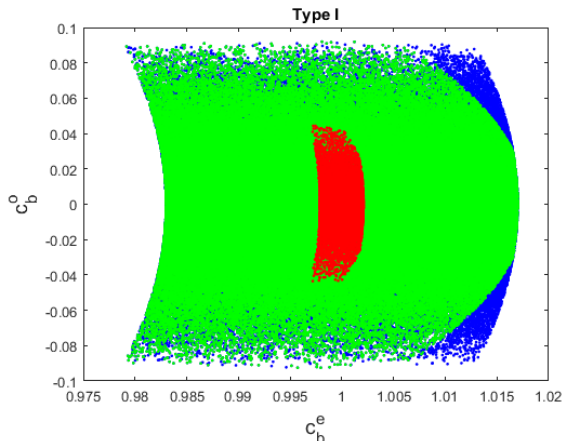
Figure 1: Yukawa couplings c_b^o vs. c_b^e (right) for the C2HDM Type I. The blue points are for $Sc1$ but without the constraints from κ_{Hgg} and $\kappa_{H\gamma\gamma}$; the green points are for $Sc1$ including κ_{Hgg} and the red points are for $Sc3$ including κ_{Hgg} and $\kappa_{H\gamma\gamma}$.

We now discuss the C2HDM. This model with a CP-violating scalar shows a quite different behaviour in the four Yukawa versions of the model. In fact, the constraints act very differently in the four Yukawa versions of the model as shown in [11]. This is particularly true for the EDMs [11] - while for Type II the electron EDM constraint almost kills the pseudoscalar component of the the bbH coupling, the same is not true for the Flipped model and for the pseudoscalar component of the Higgs couplings to leptons in the Lepton Specific model. Since different Yukawa couplings enter the two-loop Barr-Zee diagrams, a small EDM can either be the result of small CP-violating Yukawa couplings or come from cancellations between diagrams. This can even allow for maximally CP-violating Yukawa couplings of the h_{125} in some

---

[4]If a dark matter candidate is present one of the $R_{ij}, j = 2, 3$, is zero.

cases [11]. We will now study the indirect constraints from CLIC on CP-violating admixtures to the 125 GeV Higgs boson and compare them to direct constraints and constraints from EDMs.

In Fig. 1 we show the pseudoscalar component of the b-quark Yukawa coupling c_b^o versus its scalar component c_b^e. As all Yukawa couplings are equal in Type I, this plot is valid for all Type I Yukawa couplings. The blue points are for $Sc1$ but without the constraints from κ_{Hgg} and $\kappa_{H\gamma\gamma}$. The green points are for $Sc1$ including κ_{Hgg} ($\kappa_{H\gamma\gamma}$ is unconstrained by $Sc1$) and the red points are for $Sc3$ including κ_{Hgg} and $\kappa_{H\gamma\gamma}$. Note that κ_{Hgg} and $\kappa_{H\gamma\gamma}$ are the only measurements of couplings that can probe the interference between Yukawa couplings (in the case of κ_{Hgg}) and between Yukawa and Higgs gauge couplings (in the case of $\kappa_{H\gamma\gamma}$). We expect all pseudoscalar (scalar) Type I Yukawa couplings to be less than roughly 5% (0.5 %) away from the SM expectation by the end of the CLIC operation. We stress that this result assumes that experiments will not see deviations from the SM.

Recently, in [24] a study was performed for a 250 GeV electron-positron collider for Higgs-strahlung events in which the Z boson decays into electrons, muons, or hadrons, and the Higgs boson decays into τ leptons, which subsequently decay into pions. The authors found that for an integrated luminosity of 2 ab^{-1}, the mixing angle between the CP-odd and CP-even components, defined as

$$\mathcal{L}_i = g\bar{\tau}\left[\cos\psi_{CP} + i\gamma_5\sin\psi_{CP}\right]\tau H_i \; , \tag{3.20}$$

could be measured to a precision of 4.3^o which means that this is the best bound if the central measured value of the angle is zero. Their result is translated into our notation via

$$\tan\psi_{CP}^\tau = \frac{c^o(H_i\bar{\tau}\tau)}{c^e(H_i\bar{\tau}\tau)} \; . \tag{3.21}$$

Taking into account the values in Fig. 1 we obtain bounds on $\psi_{CP}^{top} = \psi_{CP}^{bottom} = \psi_{CP}^\tau$, for Type I, that are of the order of 6° for CLIC@350GeV and 3° for CLIC@3TeV. Therefore the indirect bounds are of the same order of magnitude as the direct ones.
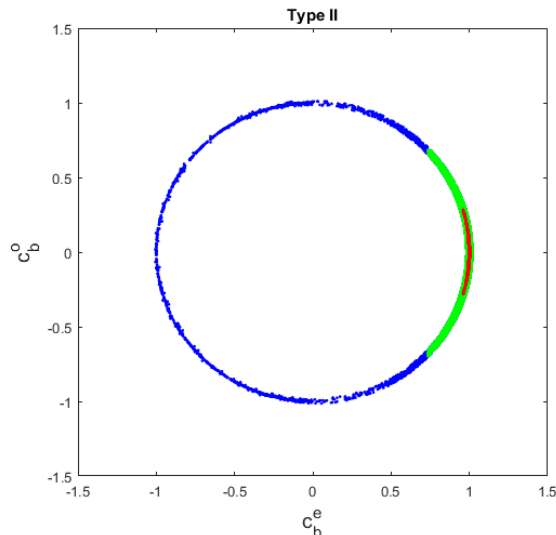
Figure 2: Yukawa couplings c_b^o vs. c_b^e (right) for the C2HDM Type II. The blue points are for $Sc1$ but without the constraints from κ_{Hgg} and $\kappa_{H\gamma\gamma}$; the green points are for $Sc1$ including κ_{Hgg} and the red points are for $Sc3$ including κ_{Hgg} and $\kappa_{H\gamma\gamma}$.

In Fig. 2 we show the pseudoscalar component of the b-quark Yukawa coupling c_b^o vs. its scalar component c_b^e. The blue points are for $Sc1$ without the constraints from κ_{Hgg} and $\kappa_{H\gamma\gamma}$. Whatever the constraint on the of tree-level couplings is, the result will always be a ring in that plane that will become increasingly thiner with growing precision. The loop induced couplings, however, are sensitive to interference between Yukawa and Higgs gauge couplings. Even for CLIC@350GeV, including the constraint on κ_{Hgg} reduces the ring to the green arch shown in the figure. By the end of the CLIC operation the arch will be further reduced to the red one. As discussed in previous works, a very precise measurement of κ_{Hgg} or $\kappa_{H\gamma\gamma}$ will kill the wrong-sign limit[5], which corresponds in the figure to $c_b^e = -1$. Now, how do these bounds compare to the direct ones from $h_{125} \to \tau^+\tau^-$? The bound on ψ_{CP}^{top} is the similar in all Yukawa types and was already discussed for Type I. In Type II $\psi_{CP}^{bottom} = \psi_{CP}^\tau$ and from Fig. 2 we obtain bounds on ψ_{CP}^{bottom} that are of the order of 30° for CLIC@350GeV and 15° for CLIC@3TeV. We conclude that for Type II the indirect bounds cannot compete with the direct ones. The EDM constraints also play a very important role in probing the CP-odd components of the couplings. In fact, in the particular scenario of the Type II C2HDM in which the lightest Higgs boson is the $125\,$GeV scalar, the bound is already constraining ψ_{CP}^{bottom} to be below 20° [11] clearly competing with the expectations for CLIC. These constraints may improve dramatically with the expected ACME II results [27].
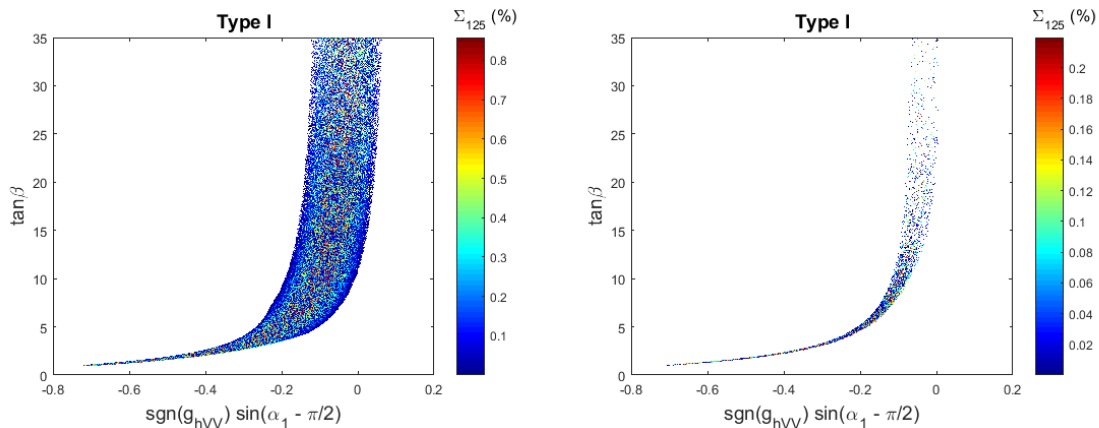
Figure 3: $\tan\beta$ as a function of $\sin(\alpha_1 - \frac{\pi}{2})$ for Type I in $Sc1$ (left) and $Sc3$ (right). The factor $-\frac{\pi}{2}$ is due to a different definition of the rotation angles relative to the 2HDM. Also shown in the colour code is the amount of singlet admixture present in h_{125}.

The predictions for the N2HDM are very similar to the ones for the 2HDM and we will discuss them together. Although the N2HDM has an extra singlet field relative to the 2HDM, the couplings to gauge bosons and fermions are very similar. For instance, for the lightest Higgs boson the couplings to massive gauge bosons are related via $g_{hVV}^{N2HDM} = \sin\alpha_2\, g_{hVV}^{2HDM}$ which results in some extra freedom for the N2HDM parameter space. In Fig. 3 we show $\tan\beta$ as a function of $\sin(\alpha_1 - \frac{\pi}{2})$ for Type I in $Sc1$ (left) and $Sc3$ (right) (the lepton-specific case behaves very similarly). The only notable difference between the N2HDM and the 2HDM is the colour bar where we show the percentage of the singlet component in the $125\,$GeV Higgs boson, $\Sigma_{125} = (R_{i3})^2$. In a previous work [28] we have shown that before the LHC run 2 the allowed admixture of the singlet was below 25% for Type I and the predictions for CLIC@350GeV and

_____

[5]The wrong sign limit refers to a Yukawa coupling that has a relative (to the coupling of the Higgs boson to the massive gauge bosons) minus sign to the corresponding SM coupling [25, 26].

CLIC@3TeV are below 0.85% and 0.22%, respectively.

As expected, the allowed parameter space gets closer and closer to the SM line, that is the line $\sin(\beta - \alpha) = 1$ (alignment limit). Note that unless one detects a new particle there is no way to find the value of $\tan\beta$ if the models are in the alignment limit. In fact, if the lightest Higgs boson is the 125 GeV one and we are in the alignment limit, $\sin(\beta - \alpha) = 1$ in the 2HDM,[6] all couplings of the 125 GeV Higgs boson to SM particles are independent of the value of $\tan\beta$ (including the triple Higgs coupling). If the 125 GeV Higgs boson is not the lightest scalar in the model, the limits change but the physics remains the same.
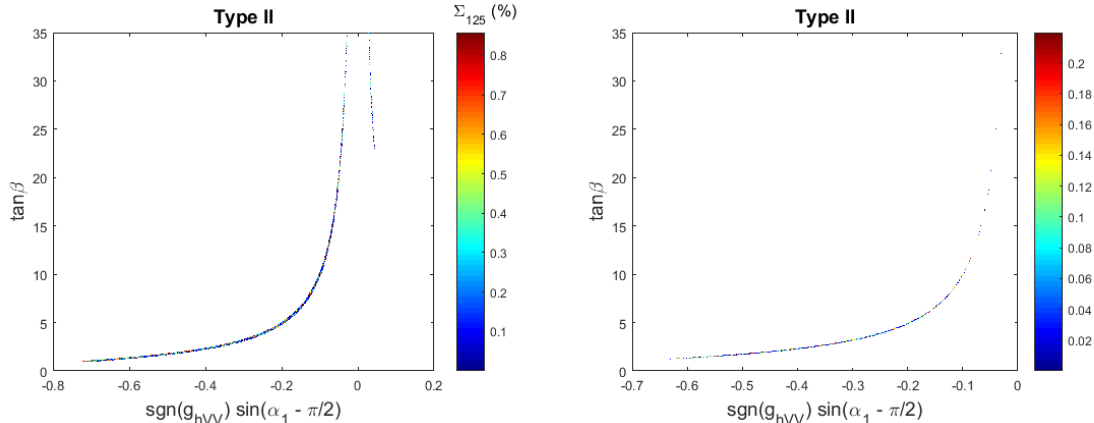
Figure 4: $\tan\beta$ as a function of $\sin(\alpha_1 - \frac{\pi}{2})$ for Type II in $Sc1$ (left) and $Sc3$ (right). The factor $-\frac{\pi}{2}$ is due to a different definition of the rotation angles relative to the 2HDM. Also shown in the colour code is the amount of singlet present in h_{125}.

In Fig. 4 we show $\tan\beta$ as a function of $\sin(\alpha_1 - \frac{\pi}{2})$ for Type II in $Sc1$ (left) and $Sc3$ (right). These are typical plots not only for a Type II N2HDM but also for a Type II 2HDM (and similar plots are obtained for the Flipped versions of both models). As previously discussed we see that the right leg, corresponding to the wrong-sign limit, is very dim in the left plot and vanishes in the right plot. Again, this is true for both the 2HDM and the N2HDM. As for the percentage of the singlet component, it was constrained to 55% for Type II N2HDM at the end of run 1 [28] and the predictions for CLIC@350GeV and CLIC@3TeV are again below about 0.85% and 0.22%, respectively.

We end this section with a discussion on the correlations between different cross section measurements for the different models. In Fig. 5 we present $\mu_t = \sigma_{\bar{t}th}^{BSM}/\sigma_{\bar{t}th}^{SM}$ as a function of $\mu_V = \sigma_{VVh}^{BSM}/\sigma_{VVh}^{SM} = \left(g_{VVh}^{BSM}/g_{VVh}^{SM}\right)^2$ for the 2HDM and N2HDM Type I and the CxSM (left) and for the 2HDM and N2HDM Type II and the NMSSM (right) for 1.4 TeV. The plots contain regions where precise measurements of deviations from the SM prediction could hint to a specific model. Take for instance the plot on the right and let us assume that the μ's could be measured with 5% precision. In this case a measurement $(\mu_t, \mu_V) = (1, 0.85)$ indicates that the model cannot be the C2HDM Type II nor the NMSSM. A measurement $(\mu_t, \mu_V) = (1.2, 1.0)$ excludes the NMSSM but not the remaining two models, in their Type II versions. Note that because $e^+e^- \to \bar{t}th$ (for which both Yukawa couplings and Higgs gauge couplings contribute)

---

[6]In the N2HDM, the alignment limit is attained for $\cos(\beta - \alpha_1)\cos\alpha_2 = 1$ (where the $\cos(\beta - \alpha_1)$ appears due to a different definition of the angle α_1 relative to the 2HDM). This means the N2HDM has SM-like couplings when $\cos(\beta - \alpha_1) = 1$ *and* $\cos\alpha_2 = 1$. In this limit the 125 GeV Higgs boson has no contribution from the singlet field.
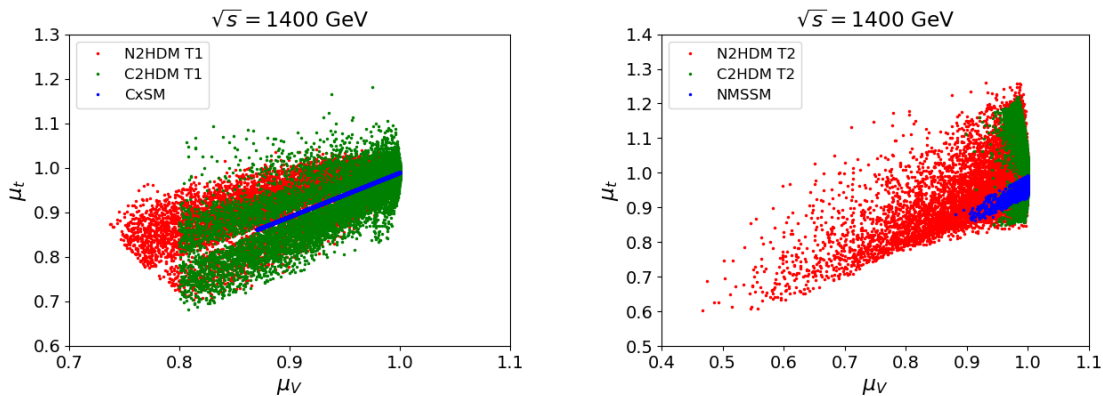
Figure 5: $\mu_t = \sigma_{\bar{t}th}^{BSM}/\sigma_{\bar{t}th}^{SM}$ as a function of $\mu_V = \sigma_{VVh}^{BSM}/\sigma_{VVh}^{SM} = \left(g_{VVh}^{BSM}/g_{VVh}^{SM}\right)^2$, where $V = W, Z$, for the 2HDM and N2HDM Type I and the CxSM (left) and for the 2HDM and N2HDM Type II and the NMSSM (right) for 1.4 TeV.

is not kinematically allowed for 350 GeV, the study of the correlations between this process and associated or W-fusion cross sections (for which only Higgs gauge couplings contribute) can only be performed for 1.4 TeV.

4   Signal Rates of the non-SM-like Higgs Bosons

In this section we present and compare the rates of the neutral non-SM-like Higgs bosons in the most relevant channels at a linear collider. We denote by $H_\downarrow$ the lighter and by $H_\uparrow$ the heavier of the two neutral non-h_{125} Higgs bosons. All signal rates are obtained by multiplying the production cross section with the corresponding branching ratio obtained from sHDECAY, C2HDM_HDECAY, N2HDECAY and NMSSMCALC. For the particular processes presented in this section, there is no distinction between particles with definite CP-numbers and CP-violating ones and they are therefore treated on equal footing. The main production processes for a Higgs boson at CLIC are associated production with a Z boson, $e^+e^- \to ZH_i$, and W-boson fusion $e^+e^- \to \nu\bar{\nu}H_i$. We will be presenting results for two centre-of-mass energies, $\sqrt{s} = 350$ GeV and $\sqrt{s} = 1.4$ TeV. In the case of the former the cross sections are comparable in the mass range presented while for the latter the W-boson fusion cross section dominates in the entire Higgs boson mass range. In order to give some meaning to the event rates presented in this section, we will use as a rough reference that at CLIC 10^{-1} fb for $Sc1$ correspond to 50 signal events and 10^{-2} fb for $Sc2$ correspond to 150 signal events.

4.1   The 350 GeV CLIC

In Fig. 6 we present the total rate for $e^+e^- \to \nu\bar{\nu}H_i \to \nu\bar{\nu}\gamma\gamma$ as a function of the Higgs boson mass for the CxSM and for the Type I versions of the N2HDM and C2HDM. Also shown is the line for a SM-like Higgs boson. The left panel contains the results for the lighter Higgs boson, $H_\downarrow$, and the right one for the heavier Higgs boson, $H_\uparrow$. The trend shown in the two plots is similar for all other final states. There is a hierarchy with the points of the N2HDM reaching the largest cross sections followed closely by the C2HDM and finally by the CxSM. This is easy to understand since the CxSM is the model with the least freedom - all couplings
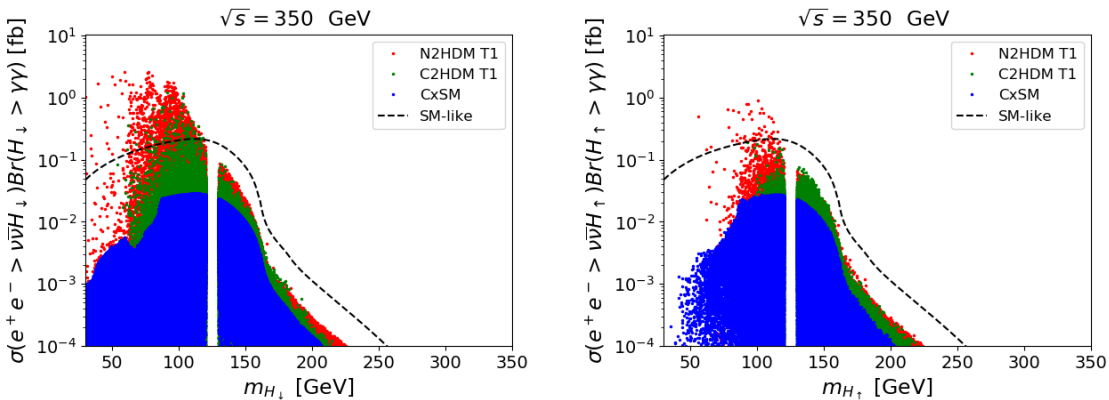
Figure 6: Total rate for $e^+e^- \to \nu\bar{\nu}H_i \to \nu\bar{\nu}\gamma\gamma$ as a function of the Higgs boson mass for $\sqrt{s} = 350$ GeV. The models presented are the CxSM and the Type I versions of the N2HDM and C2HDM. Also shown is the line for a SM-like Higgs boson. On the left panel we present the results for the lighter Higgs boson, $H_\downarrow$, and on the right we show the results for the heavier Higgs boson, $H_\uparrow$.

of the Higgs boson to SM particles are modified by the same factor - while the N2HDM is the least constrained model. This means that it is possible to distinguish between the singlet and the Type I doublet versions if a new scalar is found with a large enough rate. The $\gamma\gamma$ final state is one where the branching ratio decreases very fast with the mass. Still it is clear that there are regions of the parameter space that have large enough production rates to be detected at the 350 GeV CLIC. The behaviour seen in the plots regarding the event rates for the lighter (left) and heavier (right) scalar is the same for the remaining final states and we will only show plots for the lighter Higgs boson in the remainder of this section.

In Fig. 7 we present the total rate for $e^+e^- \to ZH_\downarrow \to Zb\bar{b}$ (left) and for $e^+e^- \to \nu\bar{\nu}H_\downarrow \to \nu\bar{\nu}b\bar{b}$ (right) as a function of $m_{H_\downarrow}$ for $\sqrt{s} = 350$ GeV, for the NMSSM and for the Type II versions of the N2HDM and C2HDM. Clearly there is plenty of parameter space to be explored in the NMSSM and even more in the Type II N2HDM. For the Type II C2HDM, as discussed in a previous work [11], the constraints are such that points with masses below about 500 GeV are excluded. Again there are regions where the models can be distinguished but not if the cross sections are too small. As expected, for this centre-of-mass energy there is not much difference between the two production processes. For a 125 GeV scalar $\sigma(e^+e^- \to ZH_i) = \sigma(e^+e^- \to \nu\bar{\nu}H_i)$ for $\sqrt{s} \approx 400$ GeV. As the scalar mass grows so does the energy for which the values of the cross sections cross. We have also checked that the behaviour does not change significantly when the Higgs boson decays to other SM particles. That is, although the rates are much higher in $H_i \to b\bar{b}$ than in $H_i \to \gamma\gamma$, the overall behaviour is the same. The highest rates are obtained in all models for the final states $b\bar{b}$, W^+W^-, ZZ and $\tau^+\tau^-$.

4.2 The 1.4 TeV CLIC

As the centre-of-mass energy rises the W-fusion process becomes the dominant one. In Fig. 8 we present the total rate for $e^+e^- \to \nu\bar{\nu}H_\downarrow \to \nu\bar{\nu}ZZ$ as a function of the lighter Higgs mass for $\sqrt{s} = 1.4$ TeV. In the left panel we show the rates for the CxSM and for the Type I N2HDM and C2HDM while in the right panel plots for the NMSSM and the Type II N2HDM and C2HDM are shown. We expect that total rates above roughly 10^{-2} fb can be explored at CLIC@1.4TeV. Hence, all models can be explored in a very large portion of their parameter space but the

11
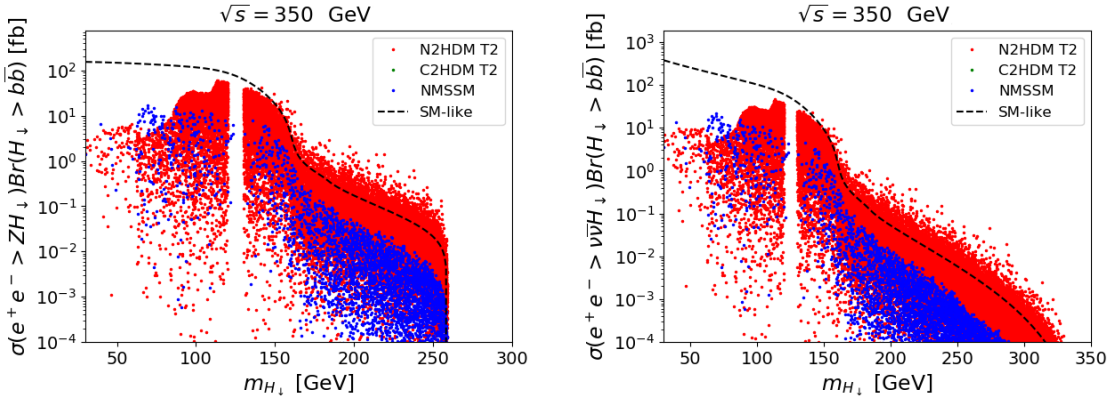
Figure 7: Total rate for $e^+e^- \to ZH_\downarrow \to Zb\bar{b}$ (left) and for $e^+e^- \to \nu\bar{\nu}H_\downarrow \to \nu\bar{\nu}b\bar{b}$ (right) as a function of $m_{H_\downarrow}$ for $\sqrt{s} = 350$ GeV. Plots are shown for the NMSSM and for the Type II versions of the N2HDM and C2HDM. Also shown is the line for a SM-like Higgs boson.
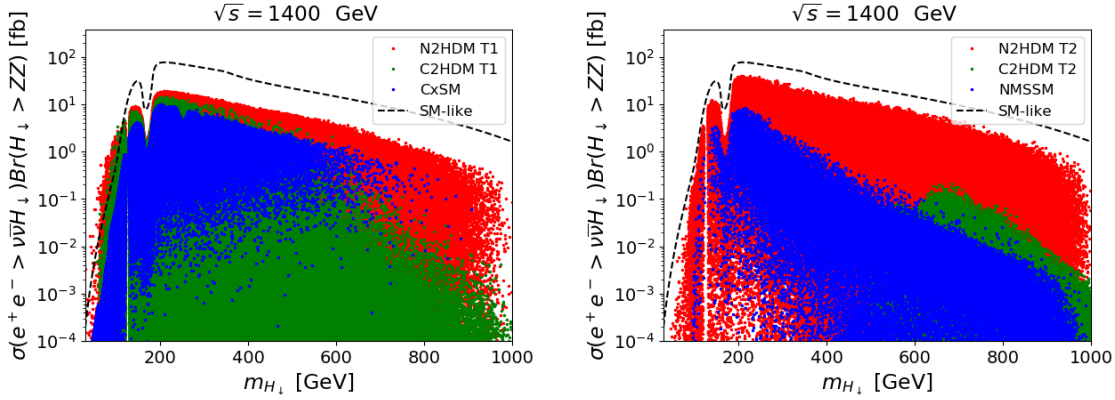
Figure 8: Total rate for $e^+e^- \to \nu\bar{\nu}H_\downarrow \to \nu\bar{\nu}ZZ$ as a function of the lighter Higgs boson mass for $\sqrt{s} = 1.4$ TeV. Left: models CxSM and Type I N2HDM and C2HDM; right: NMSSM and Type II N2HDM and C2HDM. Also shown is the line for a SM-like Higgs boson.

models are only distinguishable if large cross sections are observed. As previously discussed, the plots for the other final states do not differ much.

However, once the 350 GeV run is complete, even if no new scalar is found, the measurement of the 125 GeV Higgs couplings will be more precise which reduces the parameter space of the models. In Fig. 9 we present the total rate for $e^+e^- \to \nu\bar{\nu}H_\downarrow \to \nu\bar{\nu}ZZ$ as a function of the lighter Higgs boson mass for $\sqrt{s} = 1.4$ TeV (same as Fig. 8) including the predictions on the Higgs coupling measurements after the end of the 350 GeV run. We see that after imposing the constraints on the Higgs couplings the cross sections decrease by more than one order of magnitude. We find that the models can still be probed but are no longer distinguishable just by looking at the total rates to SM particles. Interestingly, all points from the NMMSM disappear when we impose the constraints from the 350 GeV run. This is of course related to the fact that we have used the SM central values for all predictions but it could very well be that at the end of this run we could be celebrating the discovery of a new NMSSM particle - or from any other model!
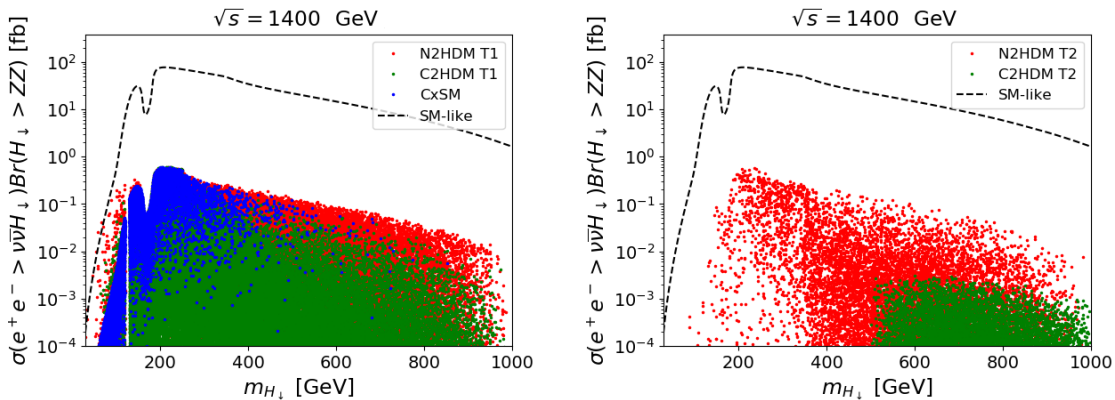
Figure 9: Same as figure 8 after imposing the final results for the 350 GeV run.

5 Conclusions

We have investigated extensions of the SM scalar sector in several specific models: the CxSM, the 2HDM, C2HDM and N2HDM in the Type I and Type II versions as well as the NMSSM. The analysis is based on three CLIC benchmarks with centre-of-mass energies of 350 GeV, 1.4 TeV and 3 TeV. For each benchmark run, the precision in the measurement of the Higgs couplings was used to study possible deviations from the – CP-even and doublet-like – expected behaviour of the discovered Higgs boson. We concluded that the constraints on the admixtures of both a singlet and a pseudoscalar component to the 125 GeV Higgs boson, improve substantially from tens of percent to well below 1% when going from the LHC to the last stage of CLIC. In fact, as shown in [28], after the LHC Run 1 the constraints on the admixtures were as shown in table 2, where Σ stands for the singlet admixture and Ψ is the pseudoscalar admixture. As noted in [28] the upper bound on Ψ for the C2HDM type II is mainly due to the EDM constraints.

Model	CxSM	C2HDM II	C2HDM I	N2HDM II	N2HDM I	NMSSM
$(\Sigma \text{ or } \Psi)_{\text{allowed}}$	11%	10%	20%	55%	25%	41%

Table 2: Allowed singlet and pseudoscalar (for the C2HDM) admixtures.

With the CLIC results the limits on the admixtures are completely dominated by the measurement of κ_{HZZ} for $Sc1$ and by κ_{HWW} for $Sc2$ and $Sc3$ through the unitarity relation

$$\kappa_{ZZ,WW}^2 + \Psi + \Sigma \leq 1\,. \tag{5.22}$$

Since this holds in all our models the constraints become independent of both model and Yukawa type and are given by

- $Sc1$: $\Sigma, \Psi < 0.85\%$ from κ_{HZZ}

- $Sc2$: $\Sigma, \Psi < 0.30\%$ from κ_{HWW}

- $Sc3$: $\Sigma, \Psi < 0.22\%$ from κ_{HWW}

In the second part of this work we investigated the potential to discover and study additional Higgs bosons at CLIC in W-boson fusion and Higgsstrahlung. We checked whether the models could be distinguished by a discovery in the first stage of CLIC. If no New Physics is found in the first stage of CLIC we discussed if the parameter space of the models still allows for large enough rates to be probed at the second stage.

- As expected the results are very similar for W-fusion and Higgsstrahlung for $\sqrt{s} = 350$ GeV. For the other two benchmark energies the W-fusion process dominates. Since the difference relative to the SM in both production processes is in the coupling hVV, $V = W, Z$, even for $\sqrt{s} = 350$ GeV, where the cross sections are of the same order, the two processes give the same information about the models.

- For $\sqrt{s} = 350$ GeV and for Type I models and CxSM, the latter is always the most constrained model as the couplings of the Higgs boson to SM particles are all modified by the same factor. Hence the Type I N2HDM and C2HDM, which in most cases are barely distinguishable, have rates that are always larger than the CxSM ones. For some final states the N2HDM rates are slightly above the C2HDM ones but always below the SM-like line, except for the $\gamma\gamma$ final states and only for Higgs boson masses below about 120 GeV. In these Type I models there are charged Higgs contributions in the $H_i \to \gamma\gamma$ loops and the charged Higgs mass is not as constrained as in the Type II models.

- For $\sqrt{s} = 350$ GeV and for Type II models and NMSSM, the C2HDM does not take part in the analysis due to the constraint on the non-125 GeV Higgs boson as previously explained. The Type II N2HDM has rates that are always above the corresponding NMSSM ones. So, it is possible to distinguish the two models in several regions of the parameter space which is expected since the N2HDM has more freedom.

- For $\sqrt{s} = 350$ GeV and for Type II models and NMSSM, the heavier neutral scalar can only be probed in the N2HDM where the rates can be up to two orders of magnitude above the SM line (these plots were not shown). CLIC can probe the lighter neutral scalar boson in both the NMSSM and the N2HDM and distinguishing the two models based on total rates alone may be possible.

- For $\sqrt{s} = 1400$ GeV the results are very similar in what regards the relative rates for the different processes. The main difference comes from imposing the predicted results for the 350 GeV run, if nothing is found and using the SM prediction as central value. This constrains the admixtures – and by unitarity the gauge couplings of the non-SM-like Higgs bosons – to tiny values identical in all models. Therefore, the models become harder to distinguish.

Acknowledgments

References

[1] ATLAS Collaboration, G. Aad *et al.*, Phys.Lett. **B716**, 1 (2012), 1207.7214.

[2] CMS Collaboration, S. Chatrchyan *et al.*, Phys.Lett. **B716**, 30 (2012), 1207.7235.

[3] D. Azevedo, P. Ferreira, M. Muhlleitner, R. Santos, and J. Wittbrodt, (2018), 1808.00755.

[4] R. Coimbra, M. O. P. Sampaio, and R. Santos, Eur. Phys. J. **C73**, 2428 (2013), 1301.2599.

[5] R. Costa, R. Guedes, M. O. P. Sampaio, and R. Santos, SCANNERS project, 2014, http://scanners.hepforge.org.

[6] R. Costa, M. Mühlleitner, M. O. P. Sampaio, and R. Santos, JHEP **06**, 034 (2016), 1512.05355.

[7] A. Djouadi, J. Kalinowski, and M. Spira, Comput. Phys. Commun. **108**, 56 (1998), hep-ph/9704448.

[8] A. Djouadi, J. Kalinowski, M. Mühlleitner, and M. Spira, (2018), 1801.09506.

[9] I. F. Ginzburg, M. Krawczyk, and P. Osland, Two Higgs doublet models with CP violation, in *Linear colliders. Proceedings, International Workshop on physics and experiments with future electron-positron linear colliders, LCWS 2002, Seogwipo, Jeju Island, Korea, August 26-30, 2002*, pp. 703–706, 2002, hep-ph/0211371, [,703(2002)].

[10] A. W. El Kaffas, P. Osland, and O. M. Ogreid, Nonlin. Phenom. Complex Syst. **10**, 347 (2007), hep-ph/0702097.

[11] D. Fontes *et al.*, JHEP **02**, 073 (2018), 1711.09419.

[12] R. Harlander, M. Mühlleitner, J. Rathsman, M. Spira, and O. Stal, (2013), 1312.5571.

[13] M. Mühlleitner, M. O. P. Sampaio, R. Santos, and J. Wittbrodt, JHEP **03**, 094 (2017), 1612.01309.

[14] I. Engeln, M. Mühlleitner, and J. Wittbrodt, (2018), 1805.00966.

[15] U. Ellwanger, J. F. Gunion, and C. Hugonie, JHEP **02**, 066 (2005), hep-ph/0406215.

[16] U. Ellwanger and C. Hugonie, Comput. Phys. Commun. **175**, 290 (2006), hep-ph/0508022.

[17] U. Ellwanger and C. Hugonie, Comput. Phys. Commun. **177**, 399 (2007), hep-ph/0612134.

[18] D. Das, U. Ellwanger, and A. M. Teixeira, Comput. Phys. Commun. **183**, 774 (2012), 1106.5633.

[19] M. Mühlleitner, A. Djouadi, and Y. Mambrini, Comput. Phys. Commun. **168**, 46 (2005), hep-ph/0311167.

[20] G. Belanger, F. Boudjema, C. Hugonie, A. Pukhov, and A. Semenov, JCAP **0509**, 001 (2005), hep-ph/0505142.

[21] J. Baglio *et al.*, Comput. Phys. Commun. **185**, 3372 (2014), 1312.4788.

[22] CLICdp, E. Sicking, Nucl. Part. Phys. Proc. **273-275**, 801 (2016).

[23] CLIC Detector and Physics Study, H. Abramowicz *et al.*, Physics at the CLIC e+e- Linear Collider – Input to the Snowmass process 2013, in *Proceedings, 2013 Community Summer Study on the Future of U.S. Particle Physics: Snowmass on the Mississippi (CSS2013): Minneapolis, MN, USA, July 29-August 6, 2013*, 2013, 1307.5288.

[24] D. Jeans and G. W. Wilson, (2018), 1804.01241.

[25] P. M. Ferreira, J. F. Gunion, H. E. Haber, and R. Santos, Phys. Rev. **D89**, 115003 (2014), 1403.4736.

[26] P. M. Ferreira, R. Guedes, M. O. P. Sampaio, and R. Santos, JHEP **12**, 067 (2014), 1409.6723.

[27] ACME, J. Baron *et al.*, New J. Phys. **19**, 073029 (2017), 1612.09318.

[28] M. Mühlleitner, M. O. P. Sampaio, R. Santos, and J. Wittbrodt, JHEP **08**, 132 (2017), 1703.07750.